DOI: 10.1021/ic100872w

Inorganic Chemistry
Article

The Triplet State of *fac*-Ir(ppy)$_3$

Thomas Hofbeck and Hartmut Yersin*

Institut für Physikalische Chemie, Universität Regensburg, D-93053 Regensburg, Germany

Received May 3, 2010

The emitting triplet state of *fac*-Ir(ppy)$_3$ (*fac*-tris(2-phenylpyridine)iridium) is studied for the first time on the basis of highly resolved optical spectra in the range of the electronic 0−0 transitions. For the compound dissolved in CH_2Cl_2 and cooled to cryogenic temperatures, three 0−0 transitions corresponding to the triplet substates I, II, and III are identified. They lie at 19 693 cm^{-1} (507.79 nm, I → 0), 19 712 cm^{-1} (507.31 nm, II → 0), and 19 863 cm^{-1} (503.45 nm, III → 0). From the large total zero-field splitting (ZFS) of 170 cm^{-1}, the assignment of the emitting triplet term as a ^{3}MLCT state (metal-to-ligand charge transfer state) is substantiated, and it is seen that spin−orbit couplings to higher lying ^{1,3}MLCT states are very effective. Moreover, the studies provide emission decay times for the three individual substates of τ_I=116 μs, τ_{II}=6.4 μs, and τ_{III}=200 ns. Further, group-theoretical considerations and investigations under application of high magnetic fields up to **B** = 12 T allow us to conclude that all three substates are nondegenerate and that the symmetry of the complex in the CH_2Cl_2 matrix cage is lower than C_3. It follows that the triplet parent term is of ^{3}A character. Studies of the emission decay time and photoluminescence quantum yield, Φ_{PL}, of Ir(ppy)$_3$ in poly(methylmethacrylate) (PMMA) in the temperature range of 1.5 ≤ T ≤ 370 K reveal average and individual radiative and nonradiative decay rates and quantum yields of the substates. In the range 80 ≤ T ≤ 370 K, Φ_{PL} is as high as almost 100%. The quantum yield Φ_{PL} drops to ∼88% when cooled to T=1.5 K. The investigations show further that the emission properties of Ir(ppy)$_3$ depend distinctly on the complex's environment or the matrix cage according to distinct changes of spin−orbit coupling effectiveness. These issues also have consequences for optimizations of the material's properties if applied as an organic light-emitting diode (OLED) emitter.

1. Introduction

Organo-transition metal compounds are of increasing interest in scientific research as well as for applications. These materials are used in dye-sensitized solar cells,[1−3] oxygen sensors,[4−6] biological labels,[7] and especially, as emitters in organic light-emitting diodes (OLEDs).[8] The pioneering investigations by Thompson and Forrest et al.,[9,10] introducing Ir(ppy)$_3$ already more than one decade ago as an electro-phosphorescent emitter, strongly stimulated the experimental[11−22] and theoretical[23−25] research in this field. The green light emitting Ir(ppy)$_3$ exhibits a very bright phosphorescence with a quantum yield of almost 100% (see below and refs 13 and 18).

*E-mail: hartmut.yersin@chemie.uni-regensburg.de.

(1) Kuciauskas, D.; Freund, M. S.; Gray, H. B.; Winkler, J. R.; Lewis, N. S. *J. Phys. Chem. B* **2001**, *105*, 392–403.
(2) O'Regan, B.; Grätzel, M. *Nature* **1991**, *353*, 737–740.
(3) Xu, Z.; Hu, B.; Howe, J. *J. Appl. Phys.* **2008**, *103*, 043909.
(4) Djurovich, P. I.; Murphy, D.; Thompson, M. E.; Hernandez, B.; Gao, R.; Hunt, P. L.; Selke, M. *Dalton Trans.* **2007**, *2007*, 3763–3770.
(5) Huynh, L.; Wang, Z.; Yang, J.; Stoeva, V.; Lough, A.; Manners, I.; Winnik, M. *Chem. Mater.* **2005**, *17*, 4765–4773.
(6) Mak, C. S. K.; Pentlehner, D. T. V.; Stich, M.; Wolfbeis, O. S.; Chan, W. K.; Yersin, H. *Chem. Mater.* **2009**, *21*, 2173–2175.
(7) Botchway, S. W.; Charnley, M.; Haycock, J. W.; Parker, A. W.; Rochester, D. L.; Weinstein, J. A.; Williams, J. A. G. *Proc. Natl. Acad. Sci. U.S.A.* **2008**, *105*, 16071–16076.
(8) *Highly Efficient OLEDs with Phosphorescent Materials*; Yersin, H., Ed.; Wiley-VCH: Weinheim, Germany, 2008.
(9) Adachi, C.; Baldo, M. A.; Forrest, S. R.; Thompson, M. E. *Appl. Phys. Lett.* **2000**, *77*, 904–906.
(10) Baldo, M. A.; Lamansky, S.; Burrows, P. E.; Thompson, M. E.; Forrest, S. R. *Appl. Phys. Lett.* **1999**, *75*, 4–6.
(11) Abe, T.; Miyazawa, A.; Konno, H.; Kawanishi, Y. *Chem. Phys. Lett.* **2010**, *491*, 199–202.
(12) Yersin, H.; Finkenzeller, W. J. In *Highly Efficient OLEDs with Phosphorescent Materials*; Yersin, H., Ed.; Wiley-VCH: Weinheim, Germany, 2008; pp 1−97.
(13) Sajoto, T.; Djurovich, P. I.; Tamayo, A. B.; Oxgaard, J.; Goddard, W. A.; Thompson, M. E. *J. Am. Chem. Soc.* **2009**, *131*, 9813–9822.
(14) Tamayo, A. B.; Alleyne, B. D.; Djurovich, P. I.; Lamansky, S.; Tsyba, I.; Ho, N. N.; Bau, R.; Thompson, M. E. *J. Am. Chem. Soc.* **2003**, *125*, 7377–7387.
(15) Ide, N.; Matsusue, N.; Kobayashi, T.; Naito, H. *Thin Solid Films* **2006**, *509*, 164–167.
(16) Bruce, D.; Richter, M. M. *Anal. Chem.* **2002**, *74*, 1340–1342.
(17) Endo, A.; Suzuki, K.; Yoshihara, T.; Tobita, S.; Yahiro, M.; Adachi, C. *Chem. Phys. Lett.* **2008**, *460*, 155–157.
(18) Goushi, K.; Kawamura, Y.; Sasabe, H.; Adachi, C. *Jpn. J. Appl. Phys.* **2004**, *43*, L937–L939.
(19) Hedley, G. J.; Ruseckas, A.; Samuel, I. D. W. *Chem. Phys. Lett.* **2008**, *450*, 292–296.
(20) Finkenzeller, W. J.; Yersin, H. *Chem. Phys. Lett.* **2003**, *377*, 299–305.
(21) Kawamura, Y.; Brooks, J.; Brown, J. J.; Sasabe, H.; Adachi, C. *Phys. Rev. Lett.* **2006**, *96*, 017404.
(22) Koide, Y.; Takahashi, S.; Vacha, M. *J. Am. Chem. Soc.* **2006**, *128*, 10990–10991.
(23) Nozaki, K. *J. Chin. Chem. Soc.* **2006**, *53*, 101–112.
(24) Jansson, E.; Minaev, B.; Schrader, S.; Agren, H. *Chem. Phys.* **2007**, *333*, 157–167.
(25) Hay, P. J. *J. Phys. Chem. A* **2002**, *106*, 1634–1641.

Published on Web 09/20/2010

Moreover, the emission decay time at ambient temperature of about 1.5 to 2 μs,[20] representing almost the radiative decay time, is relatively short for spin-forbidden triplet−singlet transitions, though an even shorter (radiative) decay time would be advantageous to restrain the roll-off of efficiency due to triplet−triplet annihilation and saturation effects. These become particularly pronounced for high-brightness OLED applications at higher current densities.[26−28] Further, $Ir(ppy)_3$ is stable even at temperatures up to at least T = 385 °C[29] and thus is well suited for vacuum deposition. Moreover, the HOMO and LUMO levels of 3.0 and 5.6 eV,[30] respectively, fit well to frequently applied hole and electron transporting matrices. This makes $Ir(ppy)_3$ highly attractive for applications in OLEDs.[9,10,26−28,31−34] Indeed, Kido et al. reported a device incorporating $Ir(ppy)_3$ with an external quantum efficiency of 29% and with a luminous efficacy of 133 lm/W at 100 cd/m^2 [28] (compare also ref 35).

Most applications of $Ir(ppy)_3$ are related to its emission properties. Hence, it is important to work out a detailed understanding of the behavior of the emitting state and the related transitions to the electronic ground state. The lowest excited state is a triplet, and thus the emission to the singlet ground state is strictly forbidden without the influence of spin−orbit coupling (SOC). This important quantum mechanical effect is induced by the 5d electrons of the heavy Ir(III) metal center. The emitting state is assigned as a ^{3}MLCT (metal-to-ligand charge transfer) state, which involves to a large extent occupied Ir 5d and unoccupied ppy π^* orbitals.[12,20,23−25,36,37] This situation is particularly advantageous for efficient SOC and thus for favorable emission properties.[12,23,38,39] Especially, SOC is responsible not only for the emission decay time and the photoluminescence quantum yield, but also for intersystem crossing (ISC) from higher lying singlets to the emitting triplet state, independently from excitations by means of optical or electron−hole recombination processes.[9,10,12,40,41] For compounds with substantial ^{3}MLCT character of the emitting state, the ISC time has been determined indirectly to be on the order of 50 fs[42] and recently also directly for $Ir(ppy)_3$ to be faster than 100 fs.[19] SOC is also crucial for another less well-known effect. The ^{3}MLCT state usually splits into three substates, the so-called zero-field splitting (ZFS). All substates are responsible for the emission properties, even at ambient temperature. For example, a large splitting shows that SOC is very effective and thus can result in a favorably short (radiative) emission decay time. On the other hand, a very large ZFS leads to a reduction of the thermal population of the highest substate and therefore might represent a limiting factor for this shortening of the decay time. Effective ISC between excited singlet(s) and the emitting triplet is also required for the triplet harvesting effect[10,12,40] and the recently discovered singlet harvesting effect,[43] which are the basis for high OLED efficiencies.

In the present investigation, we want to study properties of the emitting ^{3}MLCT state including the corresponding radiative and nonradiative transitions of $Ir(ppy)_3$ in some detail. This is reasonable, although we already proposed an energy level diagram for the triplet substates and reported individual decay dynamics.[20] These primary results were based on measurements of $Ir(ppy)_3$ dissolved in THF, for which highly resolved optical spectra could not be obtained due to large inhomogeneity and strong electron−phonon coupling effects. Thus, the reported conclusions were drawn indirectly from the emission decay behavior at different temperatures. However, we found recently that a series of Ir(III) complexes, dissolved in CH_2Cl_2, allowed us to obtain highly resolved spectra at cryogenic temperatures, in particular, in the range of the electronic 0−0 transitions.[12,38,39,44−47] Such detailed spectroscopic information gives direct insight into the electronic structures of the compound. Moreover, investigations of the photoluminescence quantum yield in combination with emission decay time measurements as a function of temperature can display radiative and nonradiative properties of the individual triplet substates. Therefore, these new challenging prospects led us to reinvestigate $Ir(ppy)_3$ in order to set a firmer basis and to obtain a deeper understanding of its properties.

2. Experimental Section

2.1. Synthesis. $Ir(ppy)_3$ was provided by Merck KGaA (Darmstadt) and was prepared with a purity degree of 99.9% according to a modified procedure (WO 02/060910), originally reported by Watts et al.[37]

2.2. Sample Preparation. $Ir(ppy)_3$ was studied in CH_2Cl_2 and THF (tetrahydrofuran), respectively, at a concentration of about 2×10^{-5} mol/L and doped in PMMA (poly(methylmethacrylate)) at a concentration well below 0.1 wt %. Solutions were degassed by several successive freeze−pump−thaw cycles applying a turbomolecular pump ($p \approx 10^{-6}$ mbar). Doped films were prepared by spin-coating and measured under nitrogen or helium atmosphere and provide well-reproducible data. PMMA as host is suitable, since it does not display any significant absorbance in the visible and near-UV range and since its glass transition temperature lies at about 378 K,[48] which permits one to carry

(26) Giebink, N. C.; Forrest, S. R. *Phys. Rev. B* **2008**, *77*, 235215.
(27) Reineke, S.; Walzer, K.; Leo, K. *Phys. Rev. B* **2007**, *75*, 125328.
(28) Tanaka, D.; Sasabe, H.; Li, Y.-J.; Su, S.-J.; Takeda, T.; Kido, J. *Jpn. J. Appl. Phys.* **2007**, *46*, L10–L12.
(29) Berger, R. J. F.; Stammler, H.-G.; Neumann, B.; Mitzel, N. W. *Eur. J. Inorg. Chem.* **2010**, *2010*, 1613–1617.
(30) Adachi, C.; Kwong, R.; Forrest, S. R. *Org. Electron.* **2001**, *2*, 37–43.
(31) He, G.; Pfeiffer, M.; Leo, K.; Hofmann, M.; Birnstock, J.; Pudzich, R.; Salbeck, J. *Appl. Phys. Lett.* **2004**, *85*, 3911–3913.
(32) Divayana, Y.; Sun, X. W. *Org. Electron.* **2010**, *11*, 67–73.
(33) Schwartz, G.; Pfeiffer, M.; Reineke, S.; Walzer, K.; Leo, K. *Adv. Mater.* **2007**, *19*, 3672–3676.
(34) Pfeiffer, M.; Forrest, S. R.; Leo, K.; Thompson, M. E. *Adv. Mater.* **2002**, *14*, 1633–1636.
(35) Birnstock, J.; Lux, A.; Ammann, M.; Wellmann, P.; Hofmann, M.; Stübinger, T. *SID 06 Dig.* **2006**, 1866–1869.
(36) Colombo, M. G.; Brunold, T. C.; Riedener, T.; Güdel, H. U.; Fortsch, M.; Buergi, H. B. *Inorg. Chem.* **1994**, *33*, 545–550.
(37) King, K. A.; Spellane, P. J.; Watts, R. J. *J. Am. Chem. Soc.* **1985**, *107*, 1431–1432.
(38) Rausch, A. F.; Homeier, H. H. H.; Yersin, H. *Top. Organomet. Chem.* **2010**, *29*, 193–235.
(39) Rausch, A. F.; Homeier, H. H. H.; Djurovich, P. I.; Thompson, M. E.; Yersin, H. *Proc. SPIE* **2007**, *6655*, 66550F.
(40) Yersin, H. *Top. Curr. Chem.* **2004**, *241*, 1–26.
(41) Adachi, C.; Baldo, M. A.; Thompson, M. E.; Forrest, S. R. *J. Appl. Phys.* **2001**, *90*, 5048–5051.
(42) Yersin, H.; Donges, D. *Top. Curr. Chem.* **2001**, *214*, 81–186.
(43) Yersin, H.; Monkowius, U. Singlet Harvesting Effect, International Patents WO 2010/006681A1 and DE 10 2008 033563A1, July 2008.
(44) Finkenzeller, W. J.; Thompson, M. E.; Yersin, H. *Chem. Phys. Lett.* **2007**, *444*, 273–279.
(45) Rausch, A. F.; Thompson, M. E.; Yersin, H. *J. Phys. Chem. A* **2009**, *113*, 5927–5932.
(46) Rausch, A. F.; Thompson, M. E.; Yersin, H. *Inorg. Chem.* **2009**, *48*, 1928–1937.
(47) Finkenzeller, W. J.; Hofbeck, T.; Thompson, M. E.; Yersin, H. *Inorg. Chem.* **2007**, *46*, 5076–5083.
(48) *Handbook of Fine Chemicals*; Sigma-Aldrich: St. Louis, Missouri, 2008.

out measurements in the large temperature range from 1.5 to ~370 K.

2.3. Spectroscopy. For absorption measurements, a Varian Cary 300 double beam spectrometer was used. Emission and excitation spectra at ambient temperature and 77 K, respectively, were measured with a Fluorolog 3-22 (Horiba Jobin Yvon) spectrophotometer. For investigations at different temperatures, a sample holder for cooling and heating, respectively, was adapted to the Fluorolog. In the range between 260 and 370 K, the sample temperature can be adjusted with an accuracy of ±0.5 K. The measurements were carried out under nitrogen atmosphere. For cryogenic temperatures, different He cryostats (Cryovac Konti Kryostat IT and Oxford Instruments cryostat) with controlled He gas flow and heating were used. Experiments under high magnetic field application were carried out with a superconducting magnet (Oxford MD 10). The spectra were recorded with an intensified CCD camera (Princeton PIMAX) or a cooled photomultiplier (RCA C7164R) in conjunction with a triple spectrograph (S&I Trivista TR 555) and a Spex 1404 double monochromator, respectively. For measurements at cryogenic temperatures and nonselective excitation, a pulsed Nd:YAG laser (λ_{exc} = 355 nm, pulse half-width < 8 ns) or a cw diode laser (λ_{exc} = 372 nm) was used, while site-selective emission and excitation spectra were obtained by use of a dye laser (Scanmate 2C, Lambda Physik) operating with Coumarin 307 and equipped with a Nd:YAG laser (λ_{pump} = 355 nm) as excitation source. Emission decay measurements were carried out using a FAST ComTec multichannel scaler PCI card with time resolution of 250 ps.

2.4. Quantum Yield Measurements. Absolute photoluminescence quantum yield measurements at ambient temperature were carried out with an integrating sphere (Labsphere with Spectralon inner surface coating) attached to the spectrophotometer Fluorolog 3-22 and with a Hamamatsu system for quantum yield measurements (C9920-02), respectively. In addition, for T = 77 K measurements of the absolute quantum yields, the Hamamatsu system[49] was equipped with a nitrogen Dewar.

The temperature dependence of the quantum yield was determined by applying a technique giving relative quantum yield data. This means that the integrated emission intensity, being proportional to the photoluminescence quantum yield, Φ_{PL}, was measured at different temperatures. Subsequently, these data were calibrated by use of the absolute Φ_{PL} values measured at ambient temperature and at 77 K. In this respect we note that the absorbance of $Ir(ppy)_3$ in PMMA is almost temperature independent at the excitation wavelength (λ_{exc} = 372 nm). This is supported by the measurement of the absolute quantum yields at 300 and 77 K and the observation that the excitation spectra measured at these temperatures do not show significant changes in the band shapes.

3. Results and Discussion

3.1. Spectroscopic Introduction. Figure 1 shows absorption, excitation, and emission spectra measured at ambient temperature and at 77 K of $Ir(ppy)_3$ in CH_2Cl_2. The absorption bands observed are assigned similarly as in ref 36. In the range below about 300 nm, the intense bands are related to spin-allowed $\pi-\pi^*$ transitions (corresponding to ligand centered states, ^{1}LC) of the cyclometalated ppy ligands. The broad and unresolved absorption band at lower energy, peaking at 376 nm, is assigned to spin-allowed d$-\pi^*$ transitions (corresponding to metal-to-ligand charge transfer states, ^{1}MLCT states), whereas absorptions at wavelengths between about 430 and 500 nm involve ^{3}MLCT states. The classifications as ^{1}LC, ^{1}MLCT, or ^{3}MLCT states should only

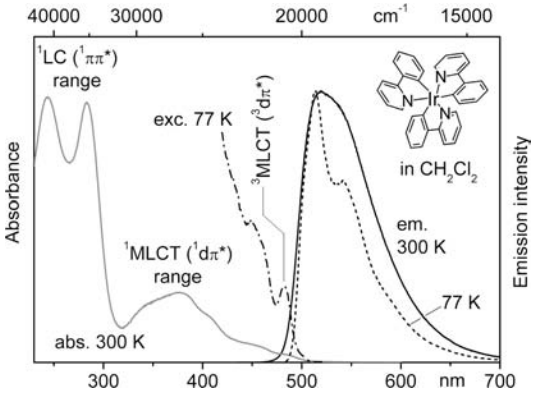

Figure 1. Emission, absorption, and excitation spectra of $Ir(ppy)_3$ in CH_2Cl_2 ($c \approx 2 \times 10^{-5}$ mol/L) measured at ambient temperature and 77 K. Emission spectra: λ_{exc} = 373 nm. Excitation spectrum: λ_{det} = 530 nm.

be taken as guidelines, since mixings between the different states by configuration interaction or spin−orbit coupling can be significant, in particular, due to the high density of states within corresponding ranges (compare refs 12 and 23−25).

The emission at ambient temperature is broad and unresolved and shows a maximum at 519 nm (~19 270 cm^{-1}). The photoluminescence quantum yield of $Ir(ppy)_3$ in degassed CH_2Cl_2 solution amounts to Φ_{PL} = (90 ± 5)% and the emission decay time is 1.6 μs. Cooling to 77 K leads to a slightly structured spectrum with a dominating peak at 514 nm (~19 460 cm^{-1}) and a satellite peak at 541 nm (~18 480 cm^{-1}). The excitation spectrum at 77 K overlaps with the emission spectrum in the range of the transitions between the electronic singlet ground state, S_0, and the emitting triplet state, ^{3}MLCT, representing the T_1 state. The Stokes shift at 77 K between the corresponding bands amounts to ~600 cm^{-1}, which we ascribe to the involvement of low-energy vibrational/phonon modes (see below).

In this study, we aimed to assign the emitting triplet state (T_1 term) in detail. It consists of triplet substates, which exhibit individual radiative and nonradiative properties. However, these data are not directly accessible from "high-temperature" measurements due to the smearing out of the spectral details according to the relatively strong host (CH_2Cl_2)−guest ($Ir(ppy)_3$) electron−phonon interactions.[12,50] Therefore, investigations at cryogenic temperatures under site-selective excitation of the compound being isolated (doped) in a suitable matrix were carried out.

3.2. Triplet Substates and Symmetry Considerations. In a neat crystalline environment, the $Ir(ppy)_3$ complex has a C_3 symmetry[51] or in a recently discovered modification a symmetry close to C_3.[29] When doped into a lower-symmetry host material, the site symmetry is necessarily also lowered. However, the extent of the distortion depends on the individual situation, and the question arises, whether the resulting effects are easily observable under a limited spectral resolution. This issue is addressed on the basis of group-theoretical considerations.

(49) Kobayashi, A.; Suzuki, K.; Yoshihara, T.; Tobita, S. *Chem. Lett.* **2010**, *39*, 282–283.

(50) Bauer, R.; Finkenzeller, W. J.; Bogner, U.; Thompson, M. E.; Yersin, H. *Org. Electron.* **2008**, *9*, 641–648.

(51) Breu, J.; Stössel, P.; Schrader, S.; Starukhin, A.; Finkenzeller, W. J.; Yersin, H. *Chem. Mater.* **2005**, *17*, 1745–1752.

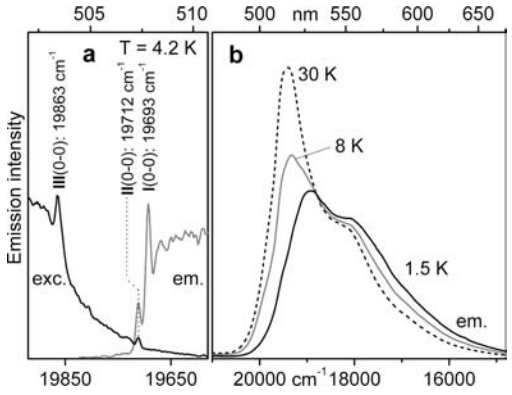

Figure 2. Emission and excitation spectra of $Ir(ppy)_3$ in CH_2Cl_2 ($c \approx 2 \times 10^{-5}$ mol/L): (a) Highly resolved spectra in the range of the electronic 0−0 transitions on an enlarged scale (excitation spectrum $\bar{\nu}_{det} = 19\,000$ cm^{-1}; emission spectrum $\bar{\nu}_{exc} = 19\,863$ cm^{-1}). Three narrow lines can be observed. They represent 0−0 transitions between the three triplet substates I, II, and III of the emitting triplet term T_1 and the ground state S_0. (b) The usually observed broad emission spectra at different temperatures (λ_{exc} = 375 nm).

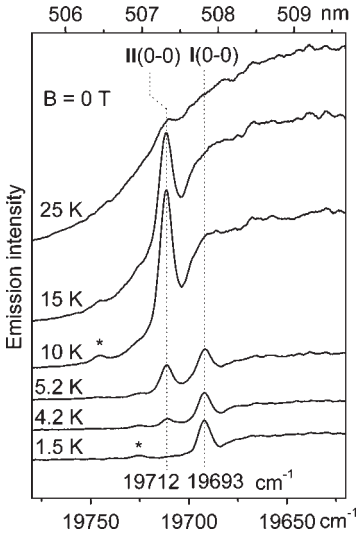

Figure 3. Emission spectra in the region of the electronic 0−0 transitions of $Ir(ppy)_3$ in CH_2Cl_2 ($c \approx 2 \times 10^{-5}$ mol/L) at different temperatures and at a magnetic field of $\mathbf{B} = 0$ T. The sample was excited resonantly into substate III (19 863 cm^{-1}). With temperature increase from 1.5 to 15 K, for example, the emission intensities of the lines at 19 712 cm^{-1} (II → 0) and at 19 693 cm^{-1} (I → 0) are strongly redistributed. The asterisks denote I → 0 and II → 0 0−0 transitions of a different, weakly emitting site.

In analogy to the discussions carried out for $[Ru(bpy)_3]^{2+}$ (see ref 52, p 175, and refs 53 and 54), the lowest triplet parent term can, in principle, result from a state of an orbitally degenerate E or a nondegenerate A representation, resulting in a ^{3}E and a ^{3}A term, respectively. Under inclusion of SOC and at a C_3 complex symmetry, the ^{3}E term splits into *four* triplet substates of E, E, A, and A representation. If the symmetry of the complex is lowered, for example, induced by the host cage or by (nonoriented) high magnetic fields, the E substates split and ^{3}E results in *six* nondegenerate triplet substates. On the other hand, the ^{3}A term splits due to SOC and at a C_3 complex symmetry into just *two* triplet substates E and A. Under symmetry reduction, the E substate will further split into two substates. Thus, at a lower symmetry than C_3, ^{3}A gives *three* triplet substates. Moreover, under application of high magnetic fields, possible E states, being present at a C_3 symmetry, split by about 1 cm^{-1}/T. Thus, the occurrence or nonoccurrence of **B**-field-induced splittings give additional insight into the properties of the triplet state.

In summary, using the information based on high-resolution studies, in particular, the number of electronic 0−0 transitions with and without application of high magnetic fields, it will be possible to classify the triplet term with respect to the relevant complex symmetry and the orbital character of the parent term. Moreover, under inclusion of further, more general systematics concerning SOC paths, it will be possible to classify the emitting triplet term also with respect to its ^{3}MLCT/^{3}LC character.

3.3. Low-Temperature Emission and High-Resolution Spectra. The emission of $Ir(ppy)_3$ dissolved (doped) in CH_2Cl_2 is, even at $T = 1.5$ K, strongly dominated by broad emission bands (Figure 2b). However, under selective excitation at 19 863 cm^{-1} (503.45 nm), weak but well-resolved electronic 0−0 transitions can be observed at the high-energy side of the broad band emission spectrum (Figure 2a). Also the excitation spectrum shows resolved peaks. In the subsequent sections, we will first discuss properties of the electronic 0−0 transitions (section 3.3.1) and then show how these are related to the broad band emission spectra (section 3.3.2).

3.3.1. Electronic 0−0 Transitions: Temperature and Magnetic Field Dependence. The combined studies of emission and excitation spectra allow us to identify three sharp electronic 0−0 transitions, which are assigned to three triplet T_1 substates I, II, and III. At $T \leq 3$ K, only substate I emits. The I → 0 0−0 transition lies at 19 693 cm^{-1} (Figures 2a and 3). This transition is only very weakly allowed. For example, the decay time of substate I is as long as $\tau_I = 116\,\mu$s (section 3.4.1). This explains, why the corresponding excitation peak could not be detected. With temperature increase, for example, to $T = 4.2$ K, another sharp line grows in at 19 712 cm^{-1} in the emission spectrum, lying 19 cm^{-1} higher in energy than the line corresponding to the I → 0 transition (Figure 3). This line is assigned to the 0−0 transition between substate II and the electronic ground state 0. The corresponding transition is significantly more allowed than the transition involving substate I. Hence, the line II → 0 appears already at relatively low temperature, for example, at $T = 4.2$ K, although a thermal population via an activation energy of 19 cm^{-1} is required. Moreover, the corresponding absorption is high enough to allow us to register the excitation peak (Figure 2a). As expected, it lies exactly (within limits of ±1 cm^{-1}) at the same energy as the corresponding emission line. The higher allowedness of the II → 0 transition is also displayed in the much shorter emission decay time of $\tau_{II} = 6.4\,\mu$s of substate II (see below). This explains why the emission line II → 0 dominates the region of the electronic origins, for example, at $T = 10$ K (Figure 3).

With additional temperature increase, the spectrum is smeared out, and above about 25 K, the resolved structure

(52) Yersin, H.; Humbs, W.; Strasser, J. *Top. Curr. Chem.* **1997**, *191*, 153–249.
(53) Ceulemans, A.; Vanquickenborne, L. G. *J. Am. Chem. Soc.* **1981**, *103*, 2238–2241.
(54) Kober, E. M.; Meyer, T. J. *Inorg. Chem.* **1982**, *21*, 3967–3977.

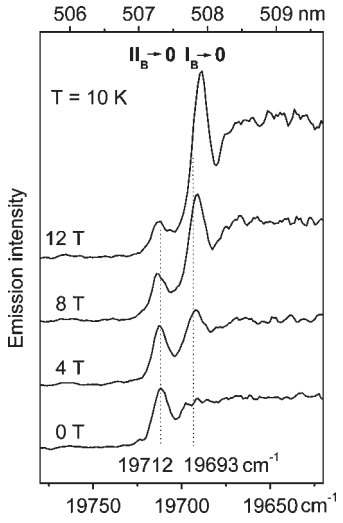

Figure 4. Emission spectra in the region of the two lower electronic 0−0 transitions of $Ir(ppy)_3$ in CH_2Cl_2 ($c \approx 2 \times 10^{-5}$ mol/L) at different magnetic fields and at $T = 10$ K. The sample was excited resonantly into substate III (19863 cm^{-1}). Under application of a magnetic field, the 0−0 transition $I_B \rightarrow 0$ is red-shifted by 4 cm^{-1} up to $\mathbf{B} = 12$ T and gains intensity with increasing field. The 0−0 transition $II_B \rightarrow 0$ shows a blue-shift of about 2 cm^{-1} up to $\mathbf{B} = 12$ T.

disappears. This behavior is ascribed to an increasing (homogeneous) coupling of the electronic structures of the doped complex to low-energy vibrational modes involving mainly modes of the complex in its matrix cage (local phonons). This so-called electron−phonon coupling is frequently responsible for the disappearance of sharp 0−0 transitions at higher temperatures. (For example, compare ref 12, p 84, and refs 50 and 55.) Therefore, the 0−0 transition corresponding to a significantly higher lying substate cannot be detected directly in an emission spectrum, if the temperature required for a thermal population of that state is higher than about 20 K. However, the corresponding transition can be observed in a low-temperature excitation spectrum. Figure 2a shows a line at 19 863 cm^{-1}, which is assigned to the 0−0 transition $0 \rightarrow$ III. It is a relatively strong transition. Its radiative allowedness is displayed in the short emission decay time of only $\tau_{III} = 200$ ns. (See section 3.4.1) No other transition that might be ascribable to an additional 0−0 transition can be observed in the energy range up to about 500 cm^{-1} from substate III. Therefore, we assign the splitting between triplet substates I and III of 170 cm^{-1} as total zero-field splitting (ZFS) of the emitting T_1 term.

Application of high magnetic fields leads to further important information about the emitting triplet term T_1. Figure 4 reproduces the emission spectra in the region of the electronic 0−0 transitions. These resolved spectra were recorded by applying selective excitation at 19 863 cm^{-1} ($0 \rightarrow$ III transition). Hence, Figure 4 displays only the emission in the range of the two lower lying electronic 0−0 transitions. The temperature of $T = 10$ K was chosen to provide sufficient thermal energy for a population also of the higher lying triplet substate II (or II_B under **B**-field application). At $\mathbf{B} = 0$ T and $T = 10$ K, the emission from substate II strongly dominates. With increasing field strength (magnetic flux density **B**), typical Zeeman effects are observed.[12,47,56−62] Due to field-induced mixings of the wave functions of the substates, substate I_B gains allowedness with respect to the transition to the electronic ground state and is red-shifted (Figure 4). For example, at $\mathbf{B} = 12$ T, the 0−0 transition $I_B \rightarrow 0$ dominates the region of the electronic origins, the emission decay time is shortened from $\tau(\mathbf{B} = 0\ T, T = 1.5\ K) = 116\ \mu s$ to $\tau(\mathbf{B} = 12\ T, T = 1.5\ K) = 31\ \mu s$, and the 0−0 transition is red-shifted by 4 cm^{-1}. Substate II_B shows a slight blue-shift of about 2 cm^{-1}, while transition $0 \rightarrow$ III, as monitored in an excitation spectrum at $T = 1.5$ K, does not exhibit any detectable shift up to $\mathbf{B} = 12$ T (not shown). These properties are typical for compounds with large zero-field split triplet terms.[52]

Importantly, none of the three electronic 0−0 transitions exhibits any splitting under application of a high magnetic field of $\mathbf{B} = 12$ T (see Figure 4 for substates I and II, the high-field excitation spectrum for transition $0 \rightarrow$ III is not reproduced). Consequently, all three substates are assigned to be nondegenerate. Thus, according to the group-theoretical considerations presented in section 3.2, it can be concluded that the $Ir(ppy)_3$ complex at the investigated site in CH_2Cl_2 is distinctly distorted from a C_3 symmetry and that the three triplet substates stem from a ^3A parent term.

In summary, the results discussed above allow us to present an energy level diagram for the emitting triplet substates of $Ir(ppy)_3$ in a CH_2Cl_2 matrix (Figure 5). In particular, the amount of total ZFS is very large with $\Delta E(ZFS) = 170$ cm^{-1}. This demonstrates efficient spin−orbit coupling to higher lying ^{1,3}MLCT states. Especially, the importance of a ^{1}MLCT admixture is displayed in the relatively short emission decay time of $\tau_{III} = 200$ ns. According to section 3.5, this decay is almost purely radiative. Moreover, it is concluded that the emitting term is largely of MLCT character (see below and refs 12, 20, 38−40, and 42). This assignment fits also to the results from theoretical investigations.[23−25]

For completeness, we will mention that the specific data presented above are primarily valid for the investigated site of $Ir(ppy)_3$ doped into CH_2Cl_2. On the other hand, nonselective excitation of $Ir(ppy)_3$ in CH_2Cl_2, giving information about the distribution of sites, shows that these exhibit almost identical photophysical data as found for the selected site. However, as will be discussed below for $Ir(ppy)_3$ doped in PMMA and THF, respectively, the triplet properties are frequently not independent of the environment of the complex (Compare also refs 46, 47, and 63).

(55) Rebane, K. K. In *Zero-Phonon Lines in Spectral Hole Burning and Photochemistry*; Sild, O., Haller, K., Eds.; Springer: Berlin, 1988.

(56) Czerwieniec, R.; Finkenzeller, W. J.; Hofbeck, T.; Starukhin, A.; Wedel, A.; Yersin, H. *Chem. Phys. Lett.* **2009**, *468*, 205–210.
(57) Braun, D.; Gallhuber, E.; Yersin, H. *Chem. Phys. Lett.* **1990**, *171*, 122–126.
(58) Dijk, N. V.; Noort, M.; Voelker, S.; Canters, G. W.; van der Waals, J. H. *Chem. Phys. Lett.* **1980**, *71*, 415–423.
(59) Chen, W.-H.; Rieckhoff, K. E.; Voigt, E.-M. *Chem. Phys.* **1985**, *95*, 123–133.
(60) Gallhuber, E.; Hensler, G.; Yersin, H. *J. Am. Chem. Soc.* **1987**, *109*, 4818–4822.
(61) Yersin, H.; Kratzer, C. *Chem. Phys. Lett.* **2002**, *362*, 365–372.
(62) Rausch, A. F.; Yersin, H. *Chem. Phys. Lett.* **2010**, *484*, 261–265.
(63) Wiedenhofer, H.; Schützenmeier, S.; von Zelewsky, A.; Yersin, H. *J. Phys. Chem.* **1995**, *99*, 13385–13391.

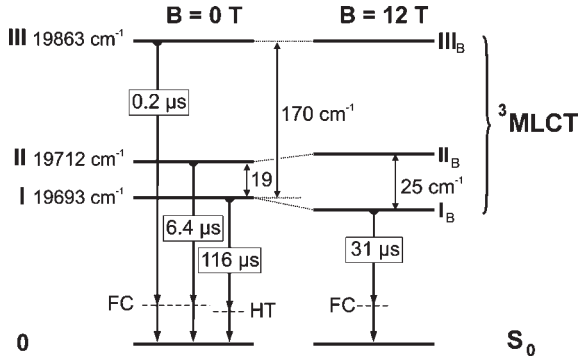

Figure 5. Energy level schemes and emission decay times for $Ir(ppy)_3$ in CH_2Cl_2 ($c \approx 2 \times 10^{-5}$ mol/L) for magnetic fields of $\mathbf{B} = 0$ T and $\mathbf{B} = 12$ T. The individual decay times result from investigations as presented in section 3.4. Representative Franck−Condon (FC) and Herzberg−Teller (HT) vibrational energy levels are also depicted.

3.3.2. Broad Band Spectra. For completeness, we briefly discuss properties of the broad band emission, although trends of the temperature dependence have already been discussed in ref 20. Figure 2b shows the corresponding spectra of $Ir(ppy)_3$ dissolved in CH_2Cl_2 at different temperatures under nonselective excitation into the ^{1}MLCT bands ($\lambda_{exc} = 375$ nm) and at a lower experimental resolution than presented in the previous section. In this situation, the very weak and narrow lines are not resolved. The spectrum at 1.5 K, resulting from the lowest substate I, shows an emission band with its maximum at about 529 nm ($\sim$18 900 cm^{-1}). Due to the relatively long decay time of $\tau_I = 116$ μs, it is indicated that the transition I $\rightarrow$ 0 is largely forbidden. This is further supported by the excitation spectrum depicted in Figure 2a. The 0−0 transition I $\rightarrow$ 0 could not be detected in contrast to the 0−0 transitions II $\rightarrow$ 0 and III $\rightarrow$ 0. It has been proposed in ref 20 that the emission process from substate I is induced by vibronic coupling (Herzberg−Teller (HT) coupling), in particular, by spin−vibronic coupling. This process opens the radiative paths to the ground state only by the involvement of specific vibrational modes. These induce couplings to higher lying singlet states, and this results in an occurrence of vibrational satellites, even when the purely electronic 0−0 transition is forbidden.[12,42,52,62,64,65] Frequently, in this case, the vibrational satellite lines are also smeared out by overlapping satellites, low-energy local phonon modes, and strong (homogeneous) electron−phonon coupling to the matrix. Thus, the corresponding band maximum appears at 529 nm. With temperature increase, substates II and III are thermally populated (Figure 5). These substates carry significantly more allowedness with respect to their 0−0 transitions to the electronic ground state than substate I. Thus, the corresponding emission is dominated by electronic 0−0 transitions and Franck−Condon active vibrational modes.[12,42,52,62,64,65] Since the vibrational energies of HT- and FC-active modes are usually different, an emission band with a blue-shifted maximum grows in near 514 nm ($\sim$19 460 cm^{-1}) (compare the 30 K spectrum in Figure 2b).

The explanation given above is further supported by the observed spectral changes under application of high magnetic fields. According to the **B**-field induced mixings of the three triplet substates, as described in section 3.3.1, the 0−0 transition from the perturbed substate I_B to the electronic ground state becomes allowed (Figures 4 and 5). Consequently, the emission spectrum changes due to the involvement of FC-active modes and becomes almost identical to the spectrum recorded at about 30 K and $\mathbf{B} = 0$ T. (Compare also ref 20 and refs 61 and 62 for background information concerning changes of vibronic coupling properties under application of high magnetic fields).

3.4. Emission Decay Dynamics. The temperature dependence of the (thermalized) emission decay time provides valuable information about the individual triplet substates. At $T = 1.5$ K, only substate I is populated. Therefore, the corresponding decay time can be determined directly. With increasing temperature, the triplet substates are populated according to the Boltzmann distribution. This prevents a direct measurement of the individual decay times of substates II and III. However, for a determination of the lifetimes of these substates, an indirect method can be applied that makes use of the temperature dependence of the experimentally accessible thermalized (averaged) emission decay time, τ_{av}. For a system of three excited substates, one obtains the expression[20,66,67]

$$\tau_{av} = \frac{1}{k_{av}} = \frac{1 + e^{-\Delta E_{I,II}/(k_B T)} + e^{-\Delta E_{I,III}/(k_B T)}}{k_I + k_{II}\, e^{-\Delta E_{I,II}/(k_B T)} + k_{III}\, e^{-\Delta E_{I,III}/(k_B T)}} \quad (1)$$

where k_I, k_{II}, and k_{III} represent the individual decay rates of the triplet substates I, II, and III, and $\Delta E_{I,II}$ and $\Delta E_{I,III}$ are the energy separations between the states; k_B is the Boltzmann constant.

3.4.1. Decay Properties of the Site-Selectively Excited $Ir(ppy)_3$. The decay behavior of $Ir(ppy)_3$ in CH_2Cl_2 was recorded in the temperature range from 1.5 to 300 K after site-selective excitation of the transition 0 $\rightarrow$ III at 19 863 cm^{-1} (Figure 6). The emission displays a monoexponential decay for all temperatures. This shows that spin−lattice relaxation processes between the substates, responsible for the thermal equilibration, are much faster than the emission decay times even at low temperatures.[52,68] Recently, the time constant of the thermal equilibration at ambient temperature was determined to about 3 ps.[19] Accordingly, the experimental decay times measured at different temperatures can be used for a fitting procedure applying eq 1. By carrying out this fit with fixed energy separations of $\Delta E_{I,II} = 19$ cm^{-1} and $\Delta E_{I,III} = 170$ cm^{-1}, known from the highly resolved spectra, and with a fixed decay time of $\tau_I = 116$ μs recorded at 1.5 K, the two remaining free fit parameters are determined to $\tau_{II} = 6.4$ μs and $\tau_{III} = 0.2$ μs. The resulting information is summarized in the Figures 5 and 6.

For completeness, we note that at a temperature near 176 K a crystalline/fluid phase transition occurs for the CH_2Cl_2 matrix. This may explain that the calculated average decay time at $T = 300$ K according to eq 1 of $\tau_{av} = 1$ μs deviates from the measured decay time at 300 K of $\tau = 1.6$ μs.

(64) Albrecht, A. C. *J. Chem. Phys.* **1963**, *38*, 354–365.
(65) Fischer, G. *Vibronic Coupling*; Academic Press: London, 1963.
(66) Hager, G. D.; Crosby, G. A. *J. Am. Chem. Soc.* **1975**, *97*, 7031–7037.
(67) Azumi, T.; O'Donnell, C. M.; McGlynn, S. P. *J. Chem. Phys.* **1966**, *45*, 2735–2742.
(68) Yersin, H.; Strasser, J. *Coord. Chem. Rev.* **2000**, *208*, 331–364.

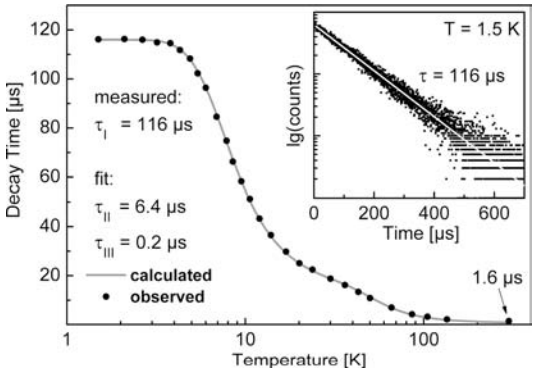

Figure 6. Temperature dependence of the emission decay time of $Ir(ppy)_3$ doped in CH_2Cl_2 ($c \approx 2 \times 10^{-5}$ mol/L) recorded after site-selective excitation at 19 863 cm^{-1} (0−0 transition 0 → III) and detection at 540 nm (~18 520 cm^{-1}). The decay at 300 K was measured in a deaerated CH_2Cl_2 solution. The decay times for the substates II and III of the T_1 state of $\tau_{II} = 6.4\ \mu s$ and $\tau_{III} = 0.2\ \mu s$ result from a fit of eq 1 to the measured decay times. Energy splittings of $\Delta E_{I,II} = 19\ cm^{-1}$ and $\Delta E_{I,III} = 170\ cm^{-1}$ as well as the decay time of $\tau_I = 116\ \mu s$, measured at $T = 1.5$ K, are kept fixed. The inset shows the decay at 1.5 K. It is monoexponential over more than 5 decay times. These data are also summarized in Figure 5.

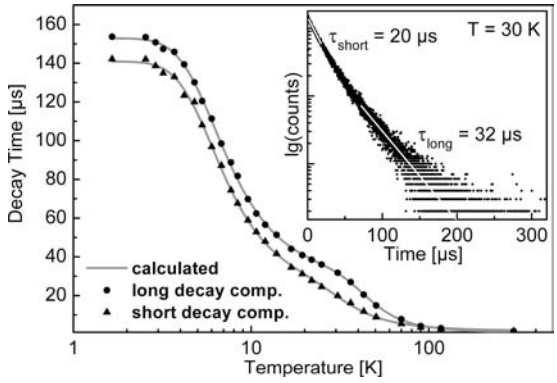

Figure 7. Temperature dependence of the emission decay time of $Ir(ppy)_3$ in THF ($c \approx 2 \times 10^{-5}$ mol/L). The inset shows, as an example, the decay behavior at 30 K. Long and short components were approximated from the measured decay curves and used for the fit procedure according to eq 1. The resulting fit parameters are given in the text and in Table 1. They characterize the spreads of the inhomogeneous distributions.

3.4.2. Matrix Dependence of Emission Decay Times and Zero-Field Splittings of $Ir(ppy)_3$. The zero-field splitting of 170 cm^{-1}, determined for $Ir(ppy)_3$ in CH_2Cl_2 (Figure 5), is significantly larger than the value of $\Delta E_{I,III} = 83\ cm^{-1}$ reported earlier[20] for $Ir(ppy)_3$ in THF. Therefore, we reinvestigate the emission properties of $Ir(ppy)_3$ dissolved in a THF matrix. In this situation, highly resolved spectra could not be obtained. Therefore, only the indirect method, as described above, can be applied. However, a monoexponential decay, as expected to occur for complexes with fast relaxations between the different triplet substates, was not found. A typical decay curve is reproduced as inset of Figure 7. At the low concentration of the $Ir(ppy)_3$ dopant, an energy transfer between the different complexes, potentially causing a deviation from the monoexponential decay, is not very probable. On the other hand, a similar multiexponential behavior was observed and discussed recently for the blue light emitting Ir(4,6-dFppy)$_2$(pic) complex (FIrpic, iridium(III)bis[2-(4′,6′-difluorophenyl)pyridinato-N,C(2′)]-picolinate) also dissolved in THF.[46] According to this report, it is proposed that the $Ir(ppy)_3$ complexes experience different environments, which modify the triplet state properties. This leads to an inhomogeneous distribution of sites with different ZFS values and different emission decay times.[12,46,47,50,63] Therefore, the measured emission decay represents a superposition of different decay times that result from different sites. In a very rough approximation, one can estimate a range of ZFS parameters and of individual emission decay times simply by using a short and a long decay component, respectively, as shown in the inset of Figure 7. The corresponding values are determined for a large temperature range, and the resulting plots are fit according to eq 1. Thus, limiting data for the inhomogeneous site distribution of $Ir(ppy)_3$ are obtained. These characterize the relevant ranges for the triplet state properties. In particular, one finds a spread of ZFS energies of $13 \le \Delta E_{I,II} \le 14\ cm^{-1}$ and of $85 \le \Delta E_{I,III} \le 150\ cm^{-1}$ and a spread of decay times of $135 \le \tau_I \le 155\ \mu s$, $10 \le \tau_{II} \le 14\ \mu s$, and of $0.2 \le \tau_{III} \le 0.6\ \mu s$. (Table 1) Thus, the ZFS values determined in ref 20 for the splitting of the T_1 term can be considered as lower limit of the ZFS range.[69]

Table 1. Ranges of Inhomogeneous Distributions of Zero-Field Splittings and Emission Decay Times of $Ir(ppy)_3$ in Two Different Matrices Compared with Photophysical Data as Found for $Ir(ppy)_3$ in CH_2Cl_2

	CH_2Cl_2[a]	THF[b]	PMMA[b]
τ_I [µs]	116	135−155	151−158
τ_{II} [µs]	6.4	10−14	13−18
τ_{III} [µs]	0.2	0.25−0.6	0.32−0.34
$\Delta E_{I,II}$ [cm^{-1}]	19	13−14	12−12.4
$\Delta E_{I,III}$ [cm^{-1}]	170	85−150	114−135

[a] Site-selective excitation at $\bar{\nu}_{exc} = 19\,863\ cm^{-1}$ (503.45 nm). [b] Nonselective excitation at $\bar{\nu}_{exc} = 28\,170\ cm^{-1}$ (355 nm).

Furthermore, the decay behavior of $Ir(ppy)_3$ was also studied in PMMA. PMMA allows an investigation at an extended temperature range up to about 370 K without any phase transition.[48] In this matrix and at low temperature, the emission decay behavior is similar to that found for the THF matrix. In particular, the decay curves are not monoexponential. Hence, an analogous fit procedure, as described for $Ir(ppy)_3$ in THF, was applied. Table 1 shows the resulting ZFS values and individual decay times. As discussed above, the long and the short decay components allow us to estimate the ranges of inhomogeneous distributions of these parameters. One notices that the variation of the ZFS parameters of $Ir(ppy)_3$ in PMMA is less distinct than that in THF. In PMMA, the total ZFS $\Delta E_{I,III}$ varies from 114 to 135 cm^{-1}, whereas $\Delta E_{I,II}$ is nearly constant amounting to ~12 cm^{-1}.

The variation of photophysical properties of the different sites of $Ir(ppy)_3$ in THF or PMMA can be explained by slight shifts of the metal d orbitals and changes of the π−d separations, for example, due to matrix cage-induced geometry variations. This alters SOC strengths and thus the ZFS values and emission decay times.[12,38,39,46,47,63] It is of particular interest that the decay time of substate III varies in THF by the large factor of about 3. Obviously, the effect of mixing of singlet character to this state via

(69) For completeness, it is mentioned that the decay curves used for the fitting procedure as carried out in ref 20 were only detected up to three or four decay times. Consequently, the long decay components were lost.

SOC is exceptionally sensitive to the environment. Especially, the emission of this triplet substate III crucially determines the OLED performance due to the substate's high radiative rate of the transition to the electronic ground state. Therefore, it is suggested to optimize the system emitter complex/matrix in order to maximize the radiative rate.

3.5. Emission Quantum Yield and Radiative and Nonradiative Decay Rates. In this section, we investigate the emission quantum yield and the radiative and nonradiative decay rates of $Ir(ppy)_3$ in the temperature range of $1.5 \leq T \leq 370$ K. For this extended range, CH_2Cl_2 and THF are not suitable as matrices, since they undergo phase transitions near $T = 178$ K and $T = 165$ K, respectively.[70] Therefore, we applied PMMA as host material.

For a deeper understanding of the emission properties of $Ir(ppy)_3$, it is desirable to have information about the radiative and nonradiative rate constants for the individual transitions from the different triplet substates I, II, and III to the singlet ground state. Corresponding data can be determined from emission quantum yield measurements for the whole temperature range and by use of emission decay time constants according to the expressions given in eqs 2 and 3.

$$\tau_i = \frac{1}{k_i} = \frac{1}{k_i^{\mathrm{r}} + k_i^{\mathrm{nr}}} \tag{2}$$

k_i, k_i^{r}, and k_i^{nr} represent the total rate constant and the radiative and the nonradiative rate constants, respectively. The index i denotes the specific triplet substate i = I, II, or III.

$$\Phi_{\mathrm{PL}} = \frac{k^{\mathrm{r}}}{k^{\mathrm{r}} + k^{\mathrm{nr}}} = \frac{1}{k} k^{\mathrm{r}} = \tau k^{\mathrm{r}} \tag{3}$$

k^{r} and k^{nr} are the sums of the individual rate constants k_i^{r} and k_i^{nr}, respectively, weighted by Boltzmann factors that take the individual thermal populations of the triplet substates into account. By use of eqs 1−3, an expression for the temperature dependence of emission quantum yield involving the three individual triplet substates is obtained (compare also ref 66):

$$\Phi_{\mathrm{PL}}(T) = \frac{k_{\mathrm{I}}^{\mathrm{r}} + k_{\mathrm{II}}^{\mathrm{r}}\, \mathrm{e}^{-\Delta E_{\mathrm{I,II}}/(k_{\mathrm{B}}T)} + k_{\mathrm{III}}^{\mathrm{r}}\, \mathrm{e}^{-\Delta E_{\mathrm{I,III}}/(k_{\mathrm{B}}T)}}{k_{\mathrm{I}} + k_{\mathrm{II}}\, \mathrm{e}^{-\Delta E_{\mathrm{I,II}}/(k_{\mathrm{B}}T)} + k_{\mathrm{III}}\, \mathrm{e}^{-\Delta E_{\mathrm{I,III}}/(k_{\mathrm{B}}T)}} \tag{4}$$

Similarly as discussed with respect to eq 1, this equation implies that the relaxation between the emitting triplet substates is much faster than the individual decay times.[20,66−68] Furthermore, since usually higher lying singlet ^{1}MLCT states are excited, eq 4 is only valid under assumption of fast intersystem crossing to the emitting triplet with an efficiency of 100%. The validity of this latter condition has recently been proven experimentally.[19,21,71]

Figure 8 shows the temperature dependence of the emission quantum yield. Interestingly, the quantum yield is almost constant and amounts to 96−97% from about

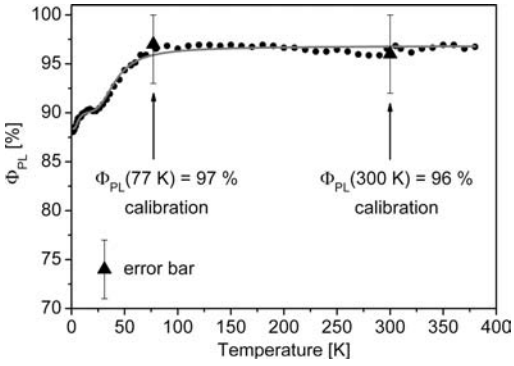

Figure 8. Temperature dependence of the emission quantum yield of $Ir(ppy)_3$ in PMMA (0.01 wt %). The experimentally determined data are calibrated using the measured absolute photoluminescence quantum yields of (96 ± 4)% at 300 K and (97 + 3/− 4)% at 77 K, respectively. The solid line represents the fit according to eq 4.

80 up to 370 K. For the temperature range of ~80 ≤ T ≤ 300 K, this result is in accordance with the data reported by Adachi et al.[18] However, below 80 K, our results differ from those of ref 18.

The quantum yield decreases from 96−97% to about 88% at 1.5 K. Between 12 and 22 K, there is a "plateau" with $\Phi_{\mathrm{PL}} \approx 90\%$. This behavior can be explained by the individual and different radiative and nonradiative rate constants of the three T_1 triplet substates. At $T = 1.5$ K, only substate I is populated. Its quantum yield amounts to $\Phi_{\mathrm{PL}} \approx 88\%$. Temperature increase leads to a population of substate II and at higher temperatures also of substate III. Between 12 and 22 K, the emission stems dominantly from substate II with a quantum yield of about 90%. At temperatures above 80 K, the emission from substate III dominates and a plateau at about 96−97% is found up to about $T = 370$ K. It is stressed that the ambient-temperature value of $\Phi_{\mathrm{PL}} = 96\%$ at an emission decay time of 1.4 μs (giving $k = 7.1 \times 10^5\ \mathrm{s}^{-1}$ and $k^{\mathrm{r}} = 6.9 \times 10^5\ \mathrm{s}^{-1}$) represents an averaged emission stemming from all three triplet sublevels.

The measured temperature dependence of the emission quantum yield $\Phi_{\mathrm{PL}}(T)$ (Figure 8) can be used to determine the radiative and nonradiative rate constants for the transitions of the individual triplet substates to the electronic ground state by applying eq 4. This equation contains eight independent variables. However, this number can be reduced. The energy splittings ($\Delta E_{\mathrm{I,II}}$, $\Delta E_{\mathrm{I,III}}$) and the rate constants k_{I}, k_{II}, and k_{III} of $Ir(ppy)_3$ in PMMA are known from Table 1. Since there, only ranges of ZFSs and emission decay times are given, we choose values lying in the center of these ranges. Thus, we can reduce the number of independent variables in eq 4 from eight to three. With the mean values of $\Delta E_{\mathrm{I,II}}$, = 12.2 cm^{-1}, $\Delta E_{\mathrm{I,III}}$ = 125 cm^{-1}, $k_{\mathrm{I}} = 1/155\ \mu\mathrm{s} = 6.5 \times 10^3\ \mathrm{s}^{-1}$, $k_{\mathrm{II}} = 1/15.5\ \mu\mathrm{s} = 6.5 \times 10^4\ \mathrm{s}^{-1}$, and $k_{\mathrm{III}} = 1/0.33\ \mu\mathrm{s} = 3.0 \times 10^6\ \mathrm{s}^{-1}$, the fit procedure applying the data of Figure 8 and using eq 4 results in the radiative decay rates of the individual triplet substates. By application of eqs 2 and 3, the corresponding individual nonradiative rate constants and quantum yields can be calculated. These data are summarized in Table 2.

Table 2 shows that the radiative rates of the three triplet substates are strongly different. The radiative process of the substate I to the singlet ground state with $k_{\mathrm{I}}^{\mathrm{r}} = 5.7 \times 10^3\ \mathrm{s}^{-1}$

(70) *CRC Handbook of Chemistry and Physics*, 83rd ed.; Lide, D. R., Ed.; CRC Press: Boca Raton, FL, 2002.

(71) Tang, K.-C.; Liu, K. L.; Chen, I.-C. *Chem. Phys. Lett.* **2004**, *386*, 437–441.

Table 2. Individual Rate Constants and Decay Times of the T_1 Substates (with i = I, II, and III) of $Ir(ppy)_3$ in PMMA.[a]

	triplet substate, i		
	I	II	III
τ_i [μs]	155	15.5	0.33
k_i [s^{-1}]	6.5×10^3	6.5×10^4	3.0×10^6
k_i^r [s^{-1}]	$(5.7 \pm 0.3) \times 10^3$	$(5.8 \pm 0.3) \times 10^4$	$(2.9 \pm 0.1) \times 10^6$
k_i^{nr} [s^{-1}]	$(8 \pm 3) \times 10^2$	$(7 \pm 3) \times 10^3$	$(1 \pm 1) \times 10^5$
$\Phi_{PL}(i)$ [%]	88 ± 4	90 ± 4	97 ± 3

[a] The individual radiative (k_i^r) and nonradiative (k_i^{nr}) rate constants and emission quantum yields ($\Phi_{PL}(i)$) result from a fit of the measured emission quantum yield $\Phi_{PL}(T)$ according to Figure 8 and eq 4 by use of mean values for the triplet substate decay times ($\tau_i = 1/k_i$) and the energy separations. These mean values are deduced from Table 1 (see the text).

displays an almost forbidden transition. In this context, it has been taken into account that the broad band emission intensity, as is applied for the estimate of the rate constants, is not carried by the electronic transition but dominantly by vibronic (HT) processes (see section 3.4.2). Therefore, substate I can be regarded as a relatively pure triplet state with very little direct SOC to higher lying singlets. On the other hand, the substates II and III exhibit radiative rates with respect to the transitions to the ground state that are greater than the rate of substate I by a factor of about 10 and 500, respectively. This is a consequence of distinctly stronger SOCs of the substates II and III to higher lying ^{1}MLCT states.[12,23,38,39] The sequence of the radiative rates $k_I^r < k_{II}^r < k_{III}^r$, as calculated by Nozaki[23] for a simplified model system of $Ir(ppy)_3$, is in accordance with the sequence as determined in this work, but the individual values differ distinctly.

The nonradiative rates of the three substates are also very different from each other. The nonradiative rate of substate I is almost one order of magnitude smaller than the nonradiative rate of substate II. This behavior is ascribed to the spin-forbiddenness of the nonradiative process from substate I to the ground state (compare refs 72 and 73). Such spin-dependent restrictions are also well-known for intersystem crossing processes in purely organic molecules.[73] With increasing singlet admixture, as is present for the substates II and III, these restrictions become less confining and thus the nonradiative processes are also more probable. However, concerning the strong increase of the calculated values of k_{II}^{nr} to k_{III}^{nr}, as given in Table 2, care is advisible. In particular, the value of k_{III}^{nr} depends on the accuracy of the Φ_{PL} calibration. For example, for the upper limit of the experimental error, the emission quantum yield could be as large as almost 100%. In this case, the nonradiative rate corresponding to substate III would become negligible. Therefore, k_{III}^{nr} can vary from 0 to 2×10^5 s^{-1}.

The individual quantum yields of the triplet substates display a behavior according to the individual radiative rates. Substate III exhibits the highest radiative rate and therefore the highest quantum yield among the triplet substates followed by substate II. The lowest individual quantum yield shows substate I.

For completeness, we note that above 370 K, the quantum yield and the emission decay time decrease (not depicted). This behavior may be due to a phase transition of PMMA, since the glass transition takes place near 378 K[48] and therefore nonradiative processes are more likely.

In summary, the emission decay time and the photoluminescence quantum yield can be well described for the large temperature range from $1.5 \leq T \leq 370$ K by three triplet substates and the singlet ground state.

4. Assignments and Conclusion

$Ir(ppy)_3$ represents one of the most attractive green light emitting compounds for OLED applications. Among several reasons, this is due to the compound's thermal stability, the exceptionally high emission quantum yield of almost 100% over the large temperature range of $\sim 80 \leq T \leq 370$ K, and the relatively short emission decay time at ambient temperature. This behavior is related to the high transition probability between the emitting triplet term T_1 and the electronic ground state. For example, the decay time of $Ir(ppy)_3$ doped in PMMA amounts to 1.4 μs at 300 K. However, these properties describe only an average behavior of the compound's features. A detailed investigation allows us to develop a much deeper understanding of the T_1 state properties.

For $Ir(ppy)_3$ in CH_2Cl_2, it is for the first time possible to resolve the 0−0 transitions of the three triplet substates I, II, and III. The splitting between the substates I and III, representing the total zero-field splitting (ZFS), is as large as 170 cm^{-1} and thus is one of the largest values measured for this kind of compounds. Applying an empirical classification, developed by Yersin et al.,[12,38−40,42,74] it can be concluded that the emitting triplet term is largely of ^{3}MLCT character. This assignment is also stated by theoretical investigations.[23−25] The large ZFS is a consequence of effective spin−orbit coupling (SOC) between the three different triplet substates and substates of higher lying ^{1,3}MLCT states. According to the extensive discussions concerning effective SOC interactions,[12,23,38,39] these ^{1,3}MLCT states have to involve other d-orbitals than that giving the emitting triplet state. Importantly, all three triplet substates experience different spin−orbit induced admixtures to higher lying singlets and, therefore, exhibit different radiative decay rates for the transitions to the electronic ground state. The corresponding rates are summarized in Table 2. For example, the radiative rate of substate III of $Ir(ppy)_3$ doped in PMMA is as large as $k_{III}^r \approx 2.9 \times 10^6$ s^{-1}, which corresponds to an emission decay time of $\tau_{III} \approx 330$ ns. Obviously, SOC is very effective with respect to substate III. Furthermore, the results show that the rate of nonradiative processes is by a factor of about 30 smaller than the radiative rate for the transition involving this state III. In particular, because of these properties of substate III, $Ir(ppy)_3$ attains its attractive emission behavior under ambient conditions. On the other hand, for the long-lived substate I with $\tau_I \approx 155$ μs (mean value in PMMA) and only little SOC to higher lying singlets, the situation concerning the nonradiative deactivation is slightly different. The radiative decay rate of $k_I^r \approx 5.7 \times 10^3$ s^{-1} is only about seven times larger than the nonradiative rate. Hence, with temperature decrease below $T = 80$ K, the emission quantum yield drops, and at very low temperature

(72) Hager, G. D.; Watts, R. J.; Crosby, G. A. *J. Am. Chem. Soc.* **1975**, *97*, 7037–7042.
(73) Turro, N. J. *Modern Molecular Photochemistry*; University Science Books: Sausalito, CA, 1991.
(74) Yersin, H.; Humbs, W. *Inorg. Chem.* **1999**, *38*, 5820–5831.

(T = 1.5 K), the quantum yield decreases to $\Phi_{PL} \approx 88\%$ (in PMMA). A drop of emission quantum yield at very low temperature has also been reported for $[Ru(bpy)_3]^{2+}$[66] and can be described similarly.

The possibility of resolving the electronic 0−0 transitions between the three triplet substates and the singlet ground state allows us to assign the emitting triplet term further. Group-theoretical considerations together with measurements at high magnetic fields up to **B** = 12 T show, because of the absence of any **B**-field-induced splitting, that the symmetry of $Ir(ppy)_3$ in CH_2Cl_2 is lower than C_3 and that the three ^{3}MLCT substates result from a ^{3}A parent term.

A general consideration seems to be of particular importance for applications of organo-transition metal compounds, as emitters in OLEDs, including $Ir(ppy)_3$. These emitters should exhibit an emission decay time as short as possible to reduce an efficiency drop (roll-off) induced by triplet−triplet annihilation or saturation effects at a high-brightness use or at high current densities.[26−28] This requires a high MLCT character of the emitting triplet state to allow for efficient SOC to higher lying ^{1}MLCT states. On the other hand, strong SOC is connected with a large ZFS. Moreover, mostly the energetically highest triplet substate III carries the largest radiative rate with respect to the transition to the singlet ground state. Since the emission decay, for example at T = 300 K, represents an averaged Boltzmann-weighted decay of all three triplet substates (compare eq 1), even a very short-lived substate III contributes only with a weakened importance due to its energy separation from the two other substates. This is displayed in the population ratio for the three states, amounting to I = 40%, II = 38%, and III = 22% ($Ir(ppy)_3$ in PMMA at 300 K). The two lower lying substates represent a reservoir of about 78% of the total population and thus are responsible for the relatively long decay time of τ = 1.4 μs at ambient temperature, although substate III decays in only ∼330 ns (in PMMA). Obviously, it is a challenge to overcome this general quandary. A very promising approach in this respect represents the application of the singlet harvesting strategy, as recently proposed by Yersin et al.[43]

Finally, our investigations show that the emission properties of $Ir(ppy)_3$ depend distinctly on the direct environment, that is, on the matrix cage of the emitter. For example, for $Ir(ppy)_3$ in THF, the total ZFS varies inhomogeneously distributed over a range of about 85 to 150 cm^{-1} and becomes as large as 170 cm^{-1} in CH_2Cl_2. Accordingly, the emission decay time of substate III, representing the most important substate for the radiative properties, varies between 200 and 600 ns. This behavior can be rationalized by matrix cage-induced variations of the complex's geometry, which can alter energy separations between occupied d-orbitals and d- or π-orbitals. These effects lead to shifts of the d-orbital energies and alter the d−π mixings (compare ref 46). Thus, the SOC strengths are distinctly changed, and therefore, modifications of crucial photophysical properties result. Consequently, an optimization of the OLED performance should take the immediate environment, that is, the matrix material, into deeper consideration.

Acknowledgment. The authors thank the *Bundesministerium für Bildung und Forschung* (*BMBF*) for the funding of this investigation. We thank also Dr. Philipp Stössel and the Merck KGaA for providing $Ir(ppy)_3$.